ISSN 1070-3284, Russian Journal of Coordination Chemistry, 2016, Vol. 42, No. 1, pp. 56–65. © Pleiades Publishing, Ltd., 2016.

Lanthanide Complexes with Pyridine-2,6-Dicarboxylic Acid: Synthesis, Crystal Structure, Thermal and Magnetic Properties of $[LnPDA)_2(PDAH_2)] \cdot (DMAH_2)_2(DMAH_{0.5})_2$[1]

S. Sharif[a], *, B. Khan[a], O. Şahin[b], and I. U. Khan[c]

[a] *Department of Chemistry, Lahore College for Women University, Lahore, 54000 Jail Road Lahore, Pakistan*
[b] *Sinop University, Scientific and Technological Research Application and Research Center, 57010 Sinop, Turkey*
[c] *GC Pakistan University, Materials Chemistry Laboratory, Department of Chemistry, 54000 Lahore, Pakistan*
**e-mail: mssshariflcwu@gmail.com; mssharif@gcu.edu.pk*

Received April 5, 2015

Abstract—Mild solvothermal synthesis, structures, thermal and magnetic properties of coordination complexes $[Ln(PDA)_2(PDAH_2)] \cdot (DMAH_2)_2(DMAH_{0.5})_2$(**I**–**IV**) (PDA = pyrdine-2,6-dicarboxylate anion, DMAH = dimethylamine, Ln = Ce, Nd, Sm, and Ho) are described. The DMAH molecules in **I**–**IV**, generated in situ from hydrolysis of *N*,*N*-dimethylformamide, are responsible to assemble three dimensional coordination polymers through N–H···O and C–H···O hydrogen bonds. Distorted tricapped trigonal prismatic LnO_6N_3 geometry having 14 triangular faces is attributed to mean deviation of dihedral angles while nitrogen shows fairly triangular faces having dihedral angle close to 60°C (CIF files CCDC nos. 872065 (**I**), 872070 (**II**), 872069 (**III**), and 872066 (**IV**)). Curie–Weiss law and the overall magnetic behavior are typical for the presence of antiferromagnetic exchange coupling interactions between lanthanide. Thermal decomposition analyses reveal removal of ammonia and resultant complexes showthermal stability. Complexes have been further characterized by using elemental analyzer and FT-IR spectroscopy.

DOI: 10.1134/S1070328416010048

INTRODUCTION

In supramolecular and materials chemistry, the construction of coordination polymers with multidentate oxygen donor ligands is rapidly growing area of research due to their fascinating structures and applications in gas storage and separation, magnetic and luminescence materials [1–3]. In order to design novel coordination polymers with specific structure and functions number of parameters, such as coordination geometry of ligand, polarity and pH of solution, metal to ligand ratio, reaction time and temperature can be carefully modified [4–7]. However, hydrogen bonding having directionality and strength due to strong donor groups, i.e. O–H or N–H also play a key role in crystal engineering to control and fine-tune of preferred structural topologies. These groups can be incorporated into a wide range of inorganic building blocks to construct discrete aggregates, one-dimensional, two-dimensional and three-dimensional networks and also further cross-linking resulting in networks of higher dimensionality [8–12]. Moreover based upon applications, hydrogen-bonded materials offer greater flexibility than coordinated system and allow additional properties owing to the presence of metals [8–10]. The multidentate ligands can be modified by introducing hydrogen bonding sites and in situ formation of these links can also be used as templates for synthesis of higher dimensional coordination polymers [13, 14]. In order to explore the coordination behavior of multidentate oxygen donor ligands with lanthanide [11, 12] for better understanding of hydrogen bonding interactions to generate supramolecular networks. Literature review reveals very few examples of in situ synthesis of dimethylamine ions by hydrolysis of *N*,*N*-dimethylformamide (DMF) [15–17]. We communicate herein generation of first example of dimethylamine ions and construction of higher-ordered aggregates through H-bond recognition, embedded in multiple hydrogen-bonding acceptors and donors. Coordination complexes were characterized by single X-ray diffraction, FT-IR, and elemental analysis. Moreover, thermogravimetric and magnetic properties have also been explored.

EXPERIMENTAL

Materials and measurements. All reagents were purchased commercially and used without further purification. Thermal analysis (25–1000°C) were recorded under continuous nitrogen flow, with a

[1] The article is published in the original.

ramp-rate of 10°C min^{-1} using a SDT Q600 instrument (TA Instruments, USA). Percentage detection of N, C, and H were performed on Elemental Analyzer, Vario Micro Cube, Elementar, Germany. IR spectra were recorded on PerkinElmer FT-IR 180 spectrophotometer using KBr pellets over the range of 4000–400 cm^{-1}. The temperature dependence of the magnetic susceptibilities were recorded at an applied magnetic field of 1000 Oe in the range of 5–300 K using Superconducting Quantum Interference Device (SQUID-MPMS-5, USA). The results are shown as plots of of χ_m, χ_m^{-1} and $\chi_m T$ versus T (χ_m is molar magnetic susceptibility) using Origin software [24]. The effective magnetic moment (μ_{eff}) was calculated by applying the relation $\mu_{eff} = 2.828\ (\chi_m T)^{1/2}$ in μ_B [25, 26].

Synthesis of $[Ce(PDA)_2(PDAH_2)] \cdot (DMAH_2)_2(DMAH_{0.5})_2$ (I). A mixture of $PDAH_2$ (84 mg, 0.50 mmol), 6 mL of water and 3 mL of DMF was stirred at 90°C for half an hour followed by dropwise addition of 5 mL aqueous solution of $Ce(NO_3)_3 \cdot 6H_2O$ (152 mg, 0.35 mmol). Stirring was continued to attain a clear solution, reflux the mixture for 4 h. Off-white block-like crystals slowly grew in the filtered solution as solvent evaporated over one month and recovered by filtration, rinsed with mixture of water and DMF (V: V = 70 : 30) and dried at room temperature. The yield was ~53%.

For $C_{29}H_{40}N_7O_{12}Ce$ (**I**) (M = 818.80):

anal. calcd., %:	C, 42.50;	H, 4.88;	N, 11.97.
Found, %:	C, 42.33;	H, 4.78;	N, 11.80.

IR (ν, cm^{-1}): 1585 $\nu_{as}(NH_2)$, 1617 $\nu_{as}(C{=}O)$, 1429, 1384 $\nu_s(C{=}O)$.

Synthesis of $[Nd(PDA)_2(PDAH_2)] \cdot (DMAH_2)_2(DMAH_{0.5})_2$ (II) was same as that in **I** except that $Ce(NO_3)_3 \cdot 6H_2O$ was replaced by $NdCl_3 \cdot 6H_2O$ (126 mg, 0.35 mmol). Violet block-like crystals slowly grew in the filtered solution as solvent evaporated over one month and recovered by filtration, rinsed with mixture of water and DMF (V: V = 70 : 30) and dried at room temperature. The yield was ~52%.

For $C_{29}H_{40}N_7O_{12}Nd$ (**II**) (M = 822.92)

anal. calcd., %:	C, 42.30;	H, 4.82;	N, 11.91.
Found, %:	C, 42.16;	H, 4.72;	N, 11.68.

IR (ν, cm^{-1}): 1580 $\nu_{as}(NH_2)$, 1620 $\nu_{as}(C{=}O)$, 1422, 1379 $\nu_s(C{=}O)$.

Synthesis of $[Sm(PDA)_2(PDAH_2)] \cdot (DMAH_2)_2(DMAH_{0.5})_2$ (III). $Ce(NO_3)_3 \cdot 6H_2O$ was replaced by $SmCl_3 \cdot 6H_2O$ (128 mg, 0.35 mmol). Off-white block-like crystals slowly grew in the filtered solution as solvent evaporated over one month and recovered by filtration, rinsed with mixture of water and DMF (V: V = 70 : 30) and dried at room temperature. The yield was ~48%.

For $C_{29}H_{40}N_7O_{12}Sm$ (**III**) (M = 829.03)

anal. calcd., %:	C, 41.98;	H, 4.82;	N, 11.82.
Found, %:	C, 41.76;	H, 4.72;	N, 11.64.

IR (ν, cm^{-1}): 1579 $\nu_{as}(NH_2)$, 1623 $\nu_{as}(C{=}O)$, 1424, 1382 $\nu_s(C{=}O)$.

Synthesis of $[Ho(PDA)_2(PDAH_2)] \cdot (DMAH_2)_2(DMAH_{0.5})_2$ (IV). $Ce(NO_3)_3 \cdot 6H_2O$ was replaced by $HoCl_3 \cdot 6H_2O$ (133 mg, 0.35 mmol). Off-white block-like crystals slowly grew in the filtered solution as solvent evaporated over one month and recovered by filtration, rinsed with mixture of water and DMF (V: V = 70 : 30) and dried at room temperature. The yield was ~50%.

For $C_{29}H_{40}N_7O_{12}Ho$ (**IV**) (M = 843.61)

anal. calcd., %:	C, 41.25;	H, 4.74;	N, 11.62.
Found, %:	C, 41.33;	H, 4.78;	N, 11.77.

IR (ν, cm^{-1}): 1561 $\nu_{as}(NH_2)$, 1633 $\nu_{as}(C{=}O)$, 1435, 1362 $\nu_s(C{=}O)$.

X-ray crystallography. Suitable crystals of **I**–**IV** were selected for data collection which was performed on a Bruker KAPA APEX II CCD diffractometer equipped with a graphite-monochromatic MoK_α radiation at 296 K. The structures were solved by direct methods using SHELXS-97 and CRYSTALS [18, 19] and refined by full-matrix least-squares methods on F^2 using SHELXL-97 and CRYSTALS [18, 19] from within the WINGX [20] suite of software. All non-hydrogen atoms were refined with anisotropic parameters. Water H atoms were located in a difference map and refined subject to a DFIX restraint of O–H 0.83(2) Å. The position of H atoms on dimethylamine molecules were located from different maps and then treated as riding atoms. All other H atoms were located from different maps and then treated as riding atoms with C–H distances of 0.93–0.96 Å and O–H distances of 0.82 Å. Molecular diagrams were created using MERCURY [21]. Supramolecular analyses were made and the diagrams were prepared with the aid of PLATON and CrystalMaker® [22, 23]. Details of data collection and crystal structure determinations are given in Table 1 and selected bond lengths and angles are given in Table 2.

Supplementary material has been deposited with the Cambridge Crystallographic Data Centre (CCDC nos. 872065 (**I**), 872070 (**II**), 872069 (**III**), and 872066 (**IV**); deposit@ccdc.cam.ac.uk or http://www.ccdc.cam.ac.uk).

Table 1. Crystallographic data and structure refinement parameters for complexes **I**–**IV**

Parameter	Value			
	I	**II**	**III**	**IV**
Crystal system	Orthorhombic	Orthorhombic	Orthorhombic	Orthorhombic
Space group	*Pbcn*	*Pbcn*	*Pbcn*	*Pbcn*
a, Å	17.0447(4)	17.0005(4)	16.9668(7)	16.9139(6)
b, Å	10.8225(2)	10.7721(3)	10.7400(4)	10.6377(3)
c, Å	18.4848(4)	18.5230(5)	18.5018(8)	18.6117(6)
V, Å^3	3409.82(13)	3392.14(15)	3371.5(2)	3348.71(19)
Z	4	4	4	4
ρ_c, g cm^{-1}	1.595	1.611	1.633	1.673
μ, mm^{-1}	1.41	1.60	1.81	2.44
θ Range, deg	2.5–6.0	3.1–8.3	2.2–8.2	2.3–8.3
Measured refls.	14589	5362	14059	3288
Independent reflections	3345	5362	3906	5461
R_{int}	0.027	0.001	0.018	0.001
S	1.06	1.03	1.12	1.09
R_1/wR_2	0.034/0.113	0.035/0.110	0.034/0.102	0.031/0.086
$\Delta\rho_{max}/\Delta\rho_{min}$, Å^{-3}	0.91/–0.93	0.63/–0.97	0.77/–0.89	0.52/–0.92

Table 2. Selected bond distances and angles for complexes **I**–**IV***

Bond	*d*, Å	Bond	*d*, Å	Bond	*d*, Å
		I			
N(1)–Ce(1)	2.624(4)	O(1)–Ce(1)	2.509(4)	O(5)–Ce(1)	2.509(3)
		II			
N(1)–Nd(1)	2.582(3)	O(3)–Nd(1)	2.499(3)	O(5)–Nd(1)	2.484(3)
N(2)–Nd(1)	2.588(4)	O(1)–Nd(1)	2.480(3)		
		III			
Sm(1)–O(1)	2.452(3)	Sm(1)–N(1)	2.551(4)	Sm(1)–O(5)	2.457(4)
		IV			
N(1)–Ho(1)	2.483(4)	O(1)–Ho(1)	2.401(3)	O(5)–Ho(1)	2.396(3)
Angle	ω, deg	Angle	ω, deg	Angle	ω, deg
		I			
O(1)Ce(1)O(1)^{i}	87.1(2)	O(5)Ce(1)O(3)	77.97(12)	O(1)Ce(1)N(2)	136.44(10)
O(1)^{i}Ce(1)O(5)^{i}	151.95(12)	O(5)Ce(1)O(3)^{i}	88.46(12)	N(1)Ce(1)N(2)	120.23(8)
		II			
O(5)Nd(1)O(5)^{i}	87.22(18)	O(5)Nd(1)N(2)	136.39(9)	O(1)Nd(1)O(3)	77.58(10)
N(1)Nd(1)N(1)^{i}	119.73(15)				
		III			
O(1)Sm(1)O(1)^{i}	126.30(15)	O(1)Sm(1)O(5)	78.31(12)	O(3)Sm(1)N(1)	136.16(12)
O(1)Sm(1)N(1)	135.46(12)	N(2)Sm(1)N(1)^{i}	120.16(9)	N(1)Sm(1)N(1)^{i}	119.68(17)
		IV			
O(1)Ho(1)O(1)^{i}	87.41(19)	O(1)Ho(1)O(3)	128.97(11)	O(1)Ho(1)N(1)	64.48(12)
N(1)Ho(1)N(1)^{i}	119.98(16)	O(5)Ho(1)N(1)	135.16(13)	N(1)Ho(1)N(2)	120.01(8)

* Symmetry codes: ^{i} $-x + 1, y, -z + 3/2$ (**I**, **II**); $-x + 1, y, -z + 1/2$ (**III**, **IV**).

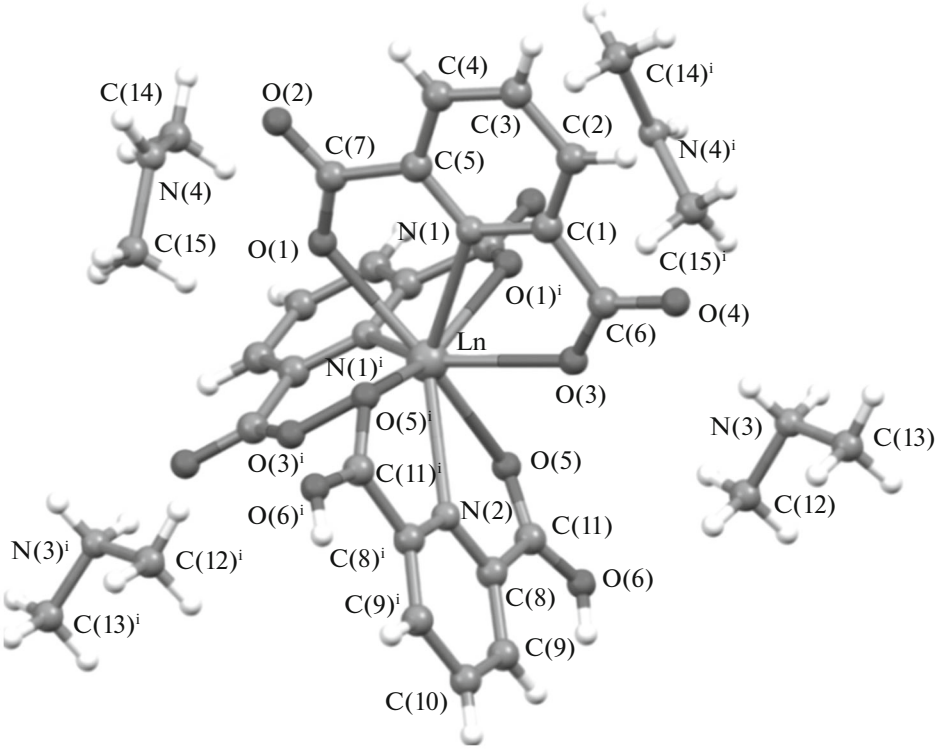

Fig. 1. The molecular structure of **I** and **IV** showing the atom numbering scheme (Ln = Ce (**I**), Ho (**IV**)). [i] $-x + 1, y, -z + 3/2$ for **I** and [i] $-x + 1, y, -z + 1/2$ for **IV**.

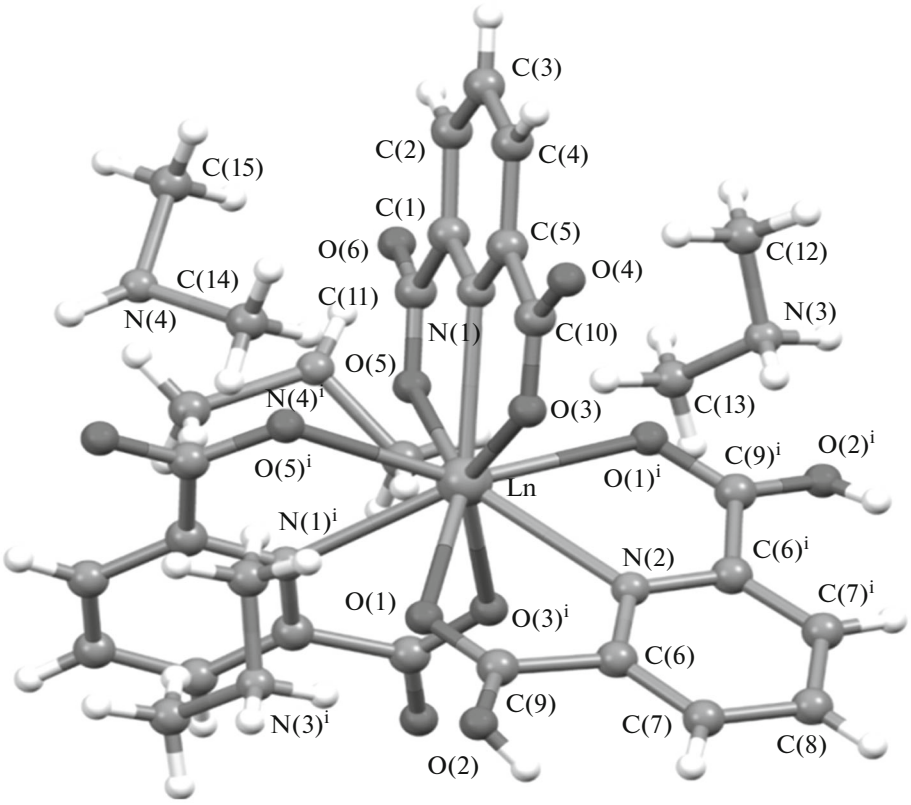

Fig. 2. The molecular structure of **II** and **III** showing the atom numbering scheme (Ln = Nd (**II**), Sm (**III**)). [i] $-x + 1, y, -z + 3/2$ for **II**; [i] $-x + 1, y, -z + 1/2$ for **III**.

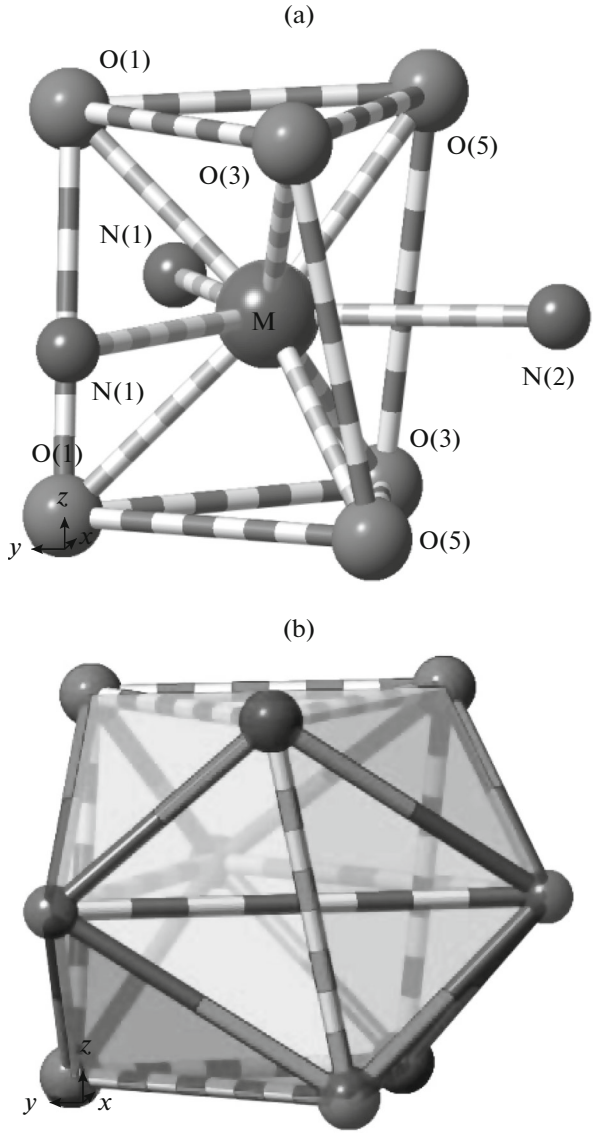

Fig. 3. Coordination geometry around Ce(III), Ho(III), Sm(III), and Nd(III) in **I**–**IV** (a); polyhedral view of coordination geometry showing triangular faces in **I**–**IV** (b).

RESULTS AND DISCUSSION

The molecular structures of **I**–**IV** with the atom numbering schemes are shown in Figs. 1 and 2. The crystallographic analyses reveal that the complexes **I**–**IV** appear very similar. Complexes **I**–**IV** crystallize in the space group *Pbcn* with $Z' = 1/2$. The asymmetric units of **I**–**IV** contain one Ln^{3+} ion (Ln = Ce (**I**), Nd (**II**), Sm (**III**), and Ho (**IV**), two non-coordinated dimethylamine ions, one pyridine-2,6-dicarboxylic ligand and one half 2,6-dicarboxylic ligand, lies about an inversion center. Each Ln^{3+} ion is located on a symmetry centre and is nine coordinated in a conventional O,N,O'-tridentate fashion by three nitrogen atoms (N(1), N(2), and N(1)^{i}) of three pyridine rings and six oxygen atoms (O(1), O(3), O(5), O(1)^{i}, O(3)^{i}, and O(5)^{i}) from six carboxylic groups. The coordination geometry around the Ln^{3+} ion in **I**–**IV** can be described as a distorted tricapped trigonal prisma, LnO_6N_3 with the N atoms serving as the caps protruding through the prismatic side-faces (Fig. 3a) having 14 triangular faces (Fig. 3b). The red dotted lines indicate the trigonal prisma of O atoms. Since the complexes are very similar, we just exampled the dihedral angles of **I** as between O(3)O(5)N(2) and O(5)O(1)N(1) triangular faces are 65.349° and 65.474° while the dihedral angles between O(5)O(3)N(2) and O(3)O(1)N(1) are 49.095° and 49.350° showing relatively distorted triangular faces. The dihedral angles between N(2)N(1)N(1)^{i}, N(1)N(1)^{i}N(2), and N(1)^{i}N(2)N(1) are 60.125°, 60.125° and 59.751° showing fairly triangular faces. The distortion in tricapped trigonal prismatic geometry is attributed to lower and upper distorted triangular faces with mean deviation of –5.413° and 10.778° from regular triangular faces. The torsion angle between O(5)–O(3)–O(5)–O(3) is –20.623°.

The Ln–O and Ln–N bond distances and NLnN, OLnO and NLnO bond angles are comparable (Table 2) to those reported for the corresponding Ce(III), Nd(III), Sm(III), and Ho(III) complexes with the pyridine-2,6-dicarboxylic ligands [11, 27–29]. The pyridine ring means planes from approximately planar with maximum deviations of 0.0048(44) Å for C(4) atom in **I**, 0.0086(37) Å for C(2) atom in **II**, 0.0053(42) Å for C(2) atom in **III** and 0.0049(42) Å for C(4) atom in **IV**, respectively.

Molecules of **I**–**IV** are linked into sheets by a combination of N–H···O and C–H···O hydrogen bonds. Strong hydrogen bonds are observed between dimethylamine ions and oxygen atoms of carboxyl groups with the N···O distances range from 2.697(7) to 3.136(6) Å. Furthermore there are also weak hydrogen bonding interactions between carbon atoms and carboxyl oxygen atoms (Table 3). Therefore, the packing diagrams of **I**–**IV** contain 3D layer filled with dimethylamine ions (Fig. 4).

In coordination complexes **I**–**IV**, Ln–O average bond lengths have been decreased from 2.509 to 2.396 (Ln–O), 2.624 to 2.482 Å for Ln–N with an increase in atomic number (Table 4). The bond lengths from cerium to holmium have been shortened by 4.50–4.04% for oxygen and 5.41–5.40% for nitrogen, which can be ascribed to 20% decrease in ionic radii of lanthanide series from lanthanum 1.061 Å to lutetium 0.848 Å [30, 31]. The small distortion in tricapped trigonal prismatic geometry is attributed to distorted triangular faces with mean deviation of –5.413° to 3.446° and 6.426° to 10.778° from regular triangular faces. The dihedral angles between nitrogen in **I**–**IV** are close to 60.0° and show fairly triangular faces. Although, the coordination number of lanthanide ions are decreasing across the series. The reported coordi-

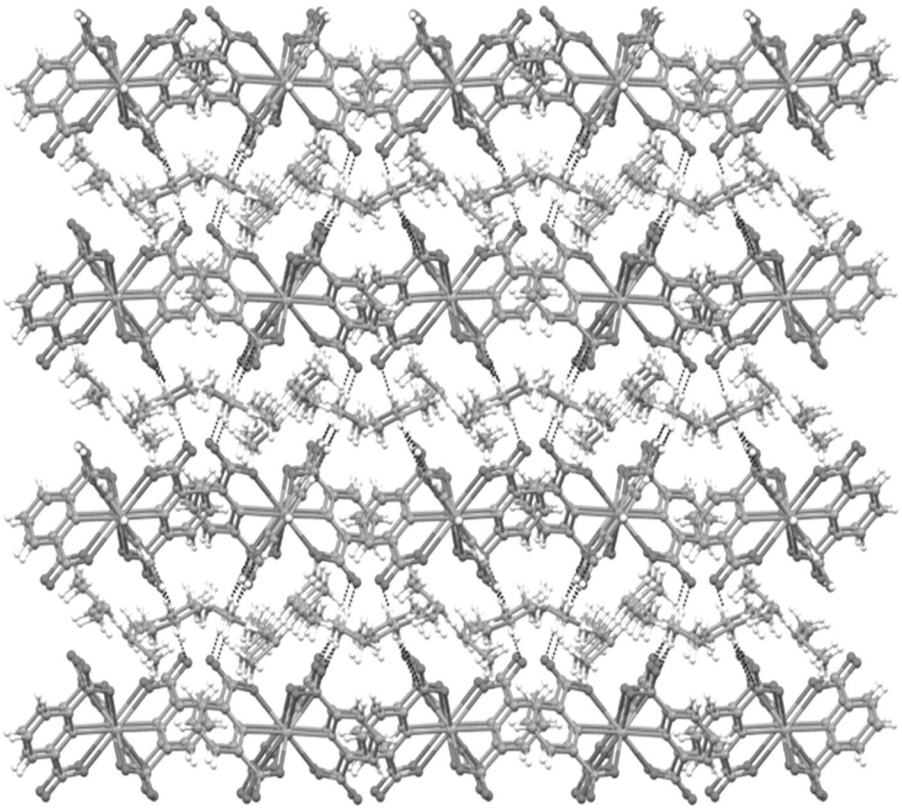

Fig. 4. An infinite 3D layers in **I**–**IV**.

nation complexes exhibit nine coordination numbers from cerium to holmium. So this effect is also attributed to electrostatic and non-directional bonding in lanthanide due to greater repulsion between ligands in the coordination sphere and therefore, geometries are basically governed by steric factors [32].

The decomposition pattern of complex **I** is illustrated in Fig. 5a. At the first stage two molecules of ammonia were released corresponding to the weight loss of 4.3% (calcd. 4.1%) from the decomposition of dimethylamine up to 90°C. TGA curve passes through a flat and the complex starts to decompose, 75.3% beyond 210°C due to successive release of organic moieties up to 980°C (calcd. 75.9%), assuming 20.4% as the final product of Ce_2O_3 (calcd. 20.0%).

The decomposition pattern of complex **III** is illustrated in Fig. 5b. At the first stage two molecules of ammonia were released corresponding to the weight loss of 4.3% (calcd. 4.1%) from the decomposition of dimethylamine up to 110°C. TGA curve passes through a flat and the complex starts to decompose, 74.1% beyond 240°C due to successive release of organic moieties up to 980°C (calcd. 74.8%), assuming 21.6% as the final product of Sm_2O_3 (calcd. 21.1%).

The decomposition pattern of complex **IV** is illustrated in Fig. 5c. At the first stage two molecules of ammonia were released corresponding to the weight loss of 3.8% (calcd. 4.0%) from the decomposition of dimethylamine up to 100°C. TGA curve passes through a flat and the complex starts to decompose, 73.4% beyond 210°C due to successive release of organic moieties up to 950°C (calcd. 73.6%), assuming 20.8% as the final product of Ho_2O_3 (calcd. 22.4%).

The magnetic behavior of **I**, **III**, and **IV** are depicted in the forms of χ_m, χ_m^{-1} and $\chi_m T$ vs. T (χ_m is molar magnetic susceptibility). A Curie–Weiss law behavior was observed for **I** above 100 K with Curie constant $C = 0.833 \pm 0.0320$ cm^3 K mol^{-1} and Weiss constant $\theta = -53.40$ K (Fig. 6a). In the high temperature end (300 K) $\chi_m T = 0.75$ cm^3 mol^{-1} K provides an effective magnetic moment μ_{eff} of 2.45 μ_B, which is slightly smaller than the expected value of 2.54 μ_B per formula for one Ce^{3+} ion of one uncoupled ($g_J = 0.85$) Ce^{3+} ion in $^2F_{5/2}$ ground state. The product of $\chi_m T$ was found to decrease with decreasing temperature to reach a final value of 0.28 cm^3 mol^{-1} K at 5 K with $\mu_{eff} = 1.50$ μ_B.

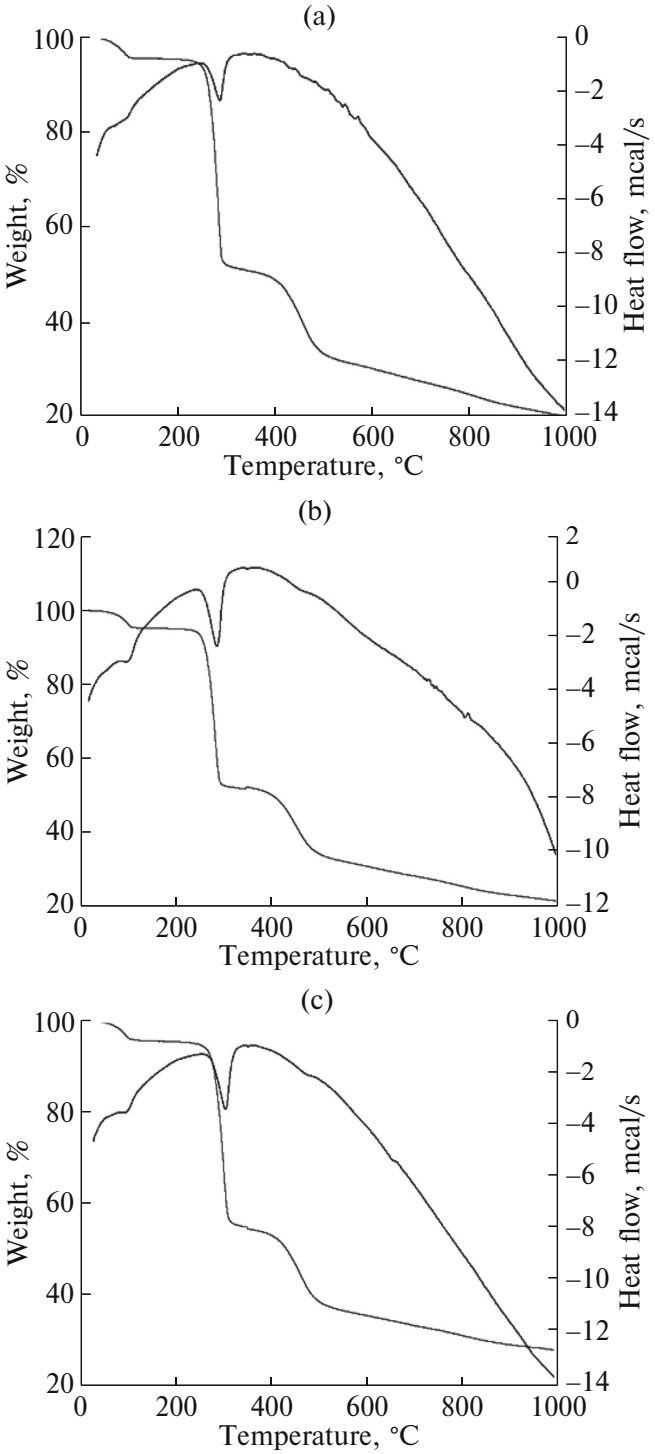

Fig. 5. TGA–DSC curves of **I** (a), **III** (b), and **IV** (c).

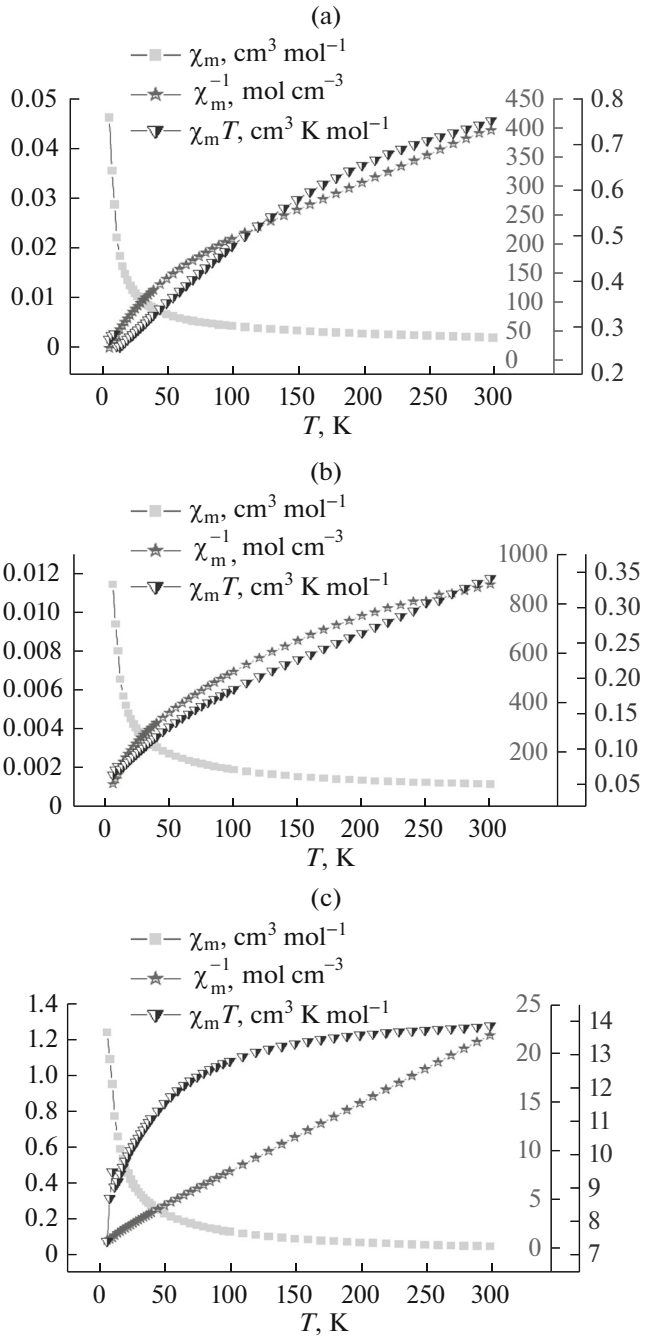

Fig. 6. Temperature dependence of χ_m, χ_m^{-1}, and $\chi_m T$ for **I** (a), **III** (b) and **IV** (c), respectively, at 1 K Oe applied field.

A Curie–Weiss law behavior was observed for **III** above 140 K with Curie constant $C = 0.157 \pm 0.0207$ cm^3 K mol^{-1} and Weiss constant $\theta = -81.56$ K (Fig. 6b). In the high temperature end (300 K) $\chi_m T = 0.1386$ cm^3 mol^{-1} K provides an effective magnetic moment μ_{eff} of 1.05 μ_B, which is slightly larger than the expected value of 0.84 μ_B per formula for one Sm^{3+} ion of one uncoupled ($g_J = 0.3$) Sm^{3+} ion in $^6H_{5/2}$ ground state. The product of $\chi_m T$ was found to decrease with decreasing temperature to reach a final value of 0.0278 cm^3 mol^{-1} K at 5 K with $\mu_{eff} = 0.47$ μ_B. The overall behavior of $\chi_m T$ with temperature and negative value of θ is typical for the presence of antiferromagnetic exchange coupling interactions.

Table 3. Geometric parameters of hydrogen bonds for complexes **I–IV***

D–H···A	Distance, Å			Angle, DHA, deg
	D–H	H···A	D···A	
		I		
N(3)–H(3*A*)···O(6)^{ii}	0.90	1.94	2.806(6)	162
N(3)–H(3*A*)···O(5)^{ii}	0.90	2.38	3.085(6)	135
N(3)–H(3*B*)···O(4)	0.90	1.83	2.723(7)	170
		II		
N(3)–H(3*A*)···O(1)^{ii}	0.97	2.36	3.098(5)	133
N(3)–H(3*A*)···O(2)^{ii}	0.97	1.85	2.791(6)	162
N(3)–H(3*B*)···O(4)^{i}	0.97	1.75	2.708(6)	169
C(14)–H(14*C*)···O(4)^{iv}	0.96	2.52	3.151(8)	123
C(15)–H(15*C*)···O(5)^{i}	0.96	2.27	3.037(6)	136
C(15)–H(15*B*)···O(2)^{iii}	0.96	2.48	3.041(6)	117
		III		
N(3)–H(3*B*)···O(2)^{ii}	0.90	1.90	2.782(7)	165
N(3)–H(3*B*)···O(1)^{ii}	0.90	2.43	3.112(6)	133
C(14)–H(14*C*)···O(5)^{iii}	0.96	2.40	3.035(7)	123
C(15)–H(15C)···O(4)^{iv}	0.96	2.44	3.166(10)	132
		IV		
N(3)–H(3*A*)···O(4)^{i}	0.97	1.74	2.695(7)	168
N(3)–H(3*B*)···O(5)^{iii}	0.97	2.42	3.136(6)	130
N(3)–H(3*B*)···O(6)^{iii}	0.97	1.80	2.749(6)	165
C(15)–H(15*A*)···O(4)^{ii}	0.96	2.59	3.176(10)	120

* Symmetry codes: ^{ii} $-x+1, -y+1, -z+1$; ^{iii} $x-1/2, y+1/2, -z+3/2$ for **I**; ^{i} $-x+1, y, -z+3/2$; ^{ii} $x, -y+1, z+1/2$; ^{iii} $-x+1, -y+1, -z+1$; ^{iv} $-x+3/2, y+1/2, z$ for **II**; ^{ii} $x, -y+1, z+1/2$; ^{iii} $-x+1, -y+1, -z+1$; ^{iv} $-x+1/2, -y+1/2, z-1/2$ for **III**; ^{i} $-x+1, y, -z+1/2$; ^{ii} $x+1/2, y-1/2, -z+1/2$; ^{iii} $x, -y+2, z-1/2$ for **IV**.

A Curie–Weiss law behavior was observed for **IV** above 20 K with Curie constant $C = 14.20 \pm 0.0002$ cm^3 K mol^{-1} and Weiss constant $\theta = -8.98$ K (Fig. 6c). In the high temperature end (300 K) $\chi_m T =$ 13.83 cm^3 mol^{-1} K provides an effective magnetic moment μ_{eff} of 10.52 μ_B, which is slightly larger than the expected value of 10.37 μ_B per formula for one Ho^{3+} ion of one uncoupled ($g_J = 1.3$) Ho^{3+} ion in $^5I_8$ ground state. The product of $\chi_m T$ was found to decrease with decreasing temperature to reach a final value of 7.43 cm^3 mol^{-1} K at 5 K with $\mu_{eff} = 7.71$ μ_B.

In this paper four novel lanthanide coordination complexes have been reported. Extensive N–H···O and C–H···O hydrogen bonds are found, leading to

Table 4. Bond lengths ranges in **I–IV**

Lanthanide	Ln–O	Ln–N
Ce	2.509(4)–2.525(3)	2.624(4)–2.625(5)
Nd	2.480(3)–2.499(3)	2.582(3)–2.587(4)
Sm	2.452(3)–2.473(3)	2.550(5)–2.551(4)
Ho	2.396(3)–2.423(3)	2.482(5)–2.483(4)

three-dimensional frameworks through different secondary building blocks. In situ generation of dimethylamine molecules demonstrate that desired hydrogen bonding sites can be incorporated by selection of appropriate solvent ratio and reaction conditions to construct higher dimensional coordination polymers and also further cross-linking of 1D and 2D in to 3D coordination polymers.

ACKNOWLEDGMENTS

The authors acknowledge the Higher Education Commission of Pakistan (HEC) for financing a visit to University of Oxford under IRSIP (HEC) and Dr. Richard Cooper, Chemical Crystallography, Chemistry Research Laboratory, Oxford, UK for helpful discussion and magnetic measurement.

REFERENCES

1. Eddaoudi, M., Kim, J., Rosi, N., et al., *Science*, 2002, vol. 295, p. 469.
2. Allendorf, M.D., Bauer, C.A., Bhakta, R.K., et al., *Chem. Soc. Rev.*, 2009, vol. 38, p. 1330.
3. Huang, Y.G., Jiang, F.L., and Hong, M.C., *Coord. Chem. Rev.*, 2009, vol. 253, p. 2814.
4. Munakata, M., Ning, G.L., Kuroda-Sowa, T., et al., *Inorg. Chem.*, 1998, vol. 37, p. 5651.
5. Losier, P. and Zaworotko, M.J., *Angew. Chem. Int. Ed.*, 1996, vol. 35, p. 2779.
6. Wen, L.L., Wang, F.-M., Leng, X.-K., et al., *J. Inorg. Organomet. Polym. Mater.*, 2010, vol. 20, p. 313.
7. Gable, R.W., Hoskins, B.F., and Robson, R., *J. Chem. Soc., Chem. Commun.*, 1990, p. 1677.
8. Desiraju, G.R., *Angew. Chem. Int. Ed.*, 1995, vol. 34, p. 2311.
9. Schauer, C.L., Matwey, E., Fowler, F.W., et al., *J. Am. Chem. Soc.*, 1997, vol. 119, p. 10245.
10. *Crystal Design: Structure and Function,* Desiraju, G.R., Ed., New York: Wiley, 2003, p. 4.
11. Khan, I.U., Sharif, S., and Sahin, O., *J. Coord. Chem.*, 2013, vol. 66, p. 3113.
12. Sharif, S., Khan, I.U., Sahin, O., et al., *J. Inorg. Organomet.*, 2012, vol. 22, p. 1165.
13. Macgillivray, L.R., *Metal-Organic Frameworks Design and Application*, Hoboken (NJ, USA): Wiley, 2010, p. 13.
14. Feng, M.-L., Xie, Z.-L., and Huang, X.-Y., *Inorg. Chem.*, 2009, vol. 48, p. 3904.
15. Feng, M.L., Kong, D.N., Xie, Z.L., et al., *Angew. Chem., Int. Ed.*, 2008, vol. 47, p. 8623.
16. Zhou, Y.-X., Cheng, G.-X., Wuc, B.-L., et al., *Acta Crystallogr., Sect. E: Struct. Rep. Online*, 2007, vol. 63, p. m2285.
17. Xu, Y.L., Han, Z., Lin, Z., et al., *Eur. J. Inorg. Chem.*, 2004, p. 4457.
18. Sheldrick, G.M., *Acta Crystallogr., Sect. A: Found. Crystallogr.*, 2008, vol. 64, p. 112.
19. Betteridge, P.W., Carruthers, J.R., Cooper, R.I., et al., *J. Appl. Cryst.*, 2003, vol. 36, p. 1487.
20. Farrugia, L.J., *J. Appl. Cryst.*, 1999, vol. 32, p. 837.
21. Macrae, C.F., Bruno, I.J., Chisholm, J.A., et al., *J. Appl. Cryst.*, 2008, vol. 41, p. 466.
22. Spek, A.L., *J. Appl. Crystallogr.*, 2003, vol. 26, p. 1.
23. *Crystal and Molecular Structures Program for Mac and Windows,* CrystalMaker® software, www.crystalmaker.com
24. *OriginPro 8 SRO*, v. 8.0724 (B724), Northampton (MA, USA), www.originLab.com
25. Blundell, S. and Thouless, D., *Magnetism in Condensed Matter*, Oxford: Oxford Univ., 2001.
26. Want, B., Ahmad, F., and Kotru, P.N., *J. Alloys Compd.*, 2008, vol. 448, p. L5.
27. Prasad, T.K. and Rajasekharan, M.V., *Cryst. Growth Des.*, 2008, vol. 8, p. 1346.
28. Wang, H.S., Zhao, B., Zhai, B., et al., *Cryst Growth Des.*, 2007, vol. 7 p. 1851.
29. Gao, H.L., Zhao, B., Zhao, X.Q., et al., *Inorg. Chem.*, 2008, vol. 47, p. 11057.
30. Karroker, D.G., *J. Chem. Ed.,* 1970, vol. 47, p. 424.
31. Keller, R.N., *J. Chem. Ed.,* 1951, p. 312.
32. *Rare Earth Coordination Chemistry Fundamentals and Applications,* Huang, C., Ed., Wiley (Asia), 2010, p. 47.